JACS
JOURNAL OF THE AMERICAN CHEMICAL SOCIETY
Article
pubs.acs.org/JACS

Tetrahedral Framework Structures: Polymorphic Phase Transition with Reorientation of Hexagonal Helical Channels in the Zintl Compound Na_2ZnSn_5 and Its Relation to $Na_5Zn_{2+x}Sn_{10-x}$

Saskia Stegmaier, Sung-Jin Kim, Alexander Henze, and Thomas F. Fässler*

Department of Chemistry, Technische Universität München, Lichtenbergstrasse 4, 85747 Garching, Germany

Supporting Information

ABSTRACT: Two modifications of the new Zintl compound Na_2ZnSn_5 were synthesized by direct reactions of the elements. *hP*-Na_2ZnSn_5, which is metastable under standard conditions, is obtained by fast cooling of a melt of stoichiometric composition. Slow cooling of such a melt or tempering of *hP*-Na_2ZnSn_5 (e.g., at 300 °C) leads to the thermodynamically stable *tI*-Na_2ZnSn_5. Both phases show an open framework structure of four-bonded Zn and Sn atoms exhibiting hexagonal helical channels in which the Na atoms are situated with disorder. Whereas the Zn−Sn network of *hP*-Na_2ZnSn_5 is analogous to known *Tr*−Sn networks (*Tr* = Ga, In), *tI*-Na_2ZnSn_5 features a closely related novel framework with a different channel structure. In the structure model for *hP*-Na_2ZnSn_5 there is only one, Zn/Sn mixed occupied, site for the framework atoms, whereas Zn and Sn are fully ordered on three sites in the case of *tI*-Na_2ZnSn_5. The phase transition from *hP*-Na_2ZnSn_5 to *tI*-Na_2ZnSn_5 was studied using high-temperature powder and single-crystal X-ray diffraction methods. Na_2ZnSn_5 is stable up to about 350 °C and does not melt congruently but decomposes to form $Na_5Zn_{2+x}Sn_{10-x}$. DFT band structure calculations (TB-LMTO-ASA) were performed with ordered model structures which were deduced from a conceivable pathway for the interconversion of the two polymorphic structures of Na_2ZnSn_5. A band gap at the Fermi level, as expected for a Zintl phase, is found for the ordered structure of *tI*-Na_2ZnSn_5. On the basis of an analysis of the relationship between the network structures of the Sn-rich Na−Zn−Sn phases, a general perspective for novel open framework structures with exclusively four-bonded atoms is given.

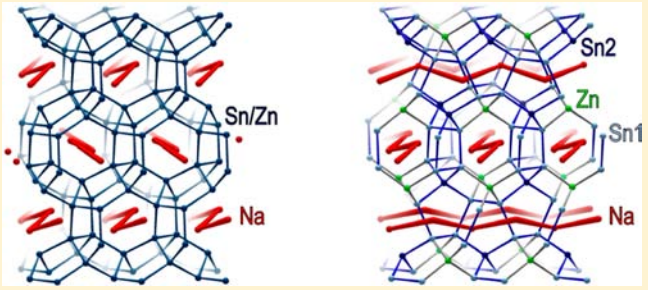

INTRODUCTION

Allotropes of the group 14 elements C, Si, Ge, and Sn represent a variety of network structures which are, conforming to the valency of the elements, exclusively built of four-connected atoms in (ideal or distorted) tetrahedral coordination environments. Due to the different electronic structures (band gaps) and the associated optophysical properties which come along with the different structure types, the investigation of novel group 14 element allotropes is of high interest. Recently new crystalline allotropes have been found experimentally; examples include *(m-)allo*-Ge[1,2] and clathrate-II Ge.[3−5] Other allotropes have been suggested theoretically.[6−12]

Four-connected network nodes can also be formed by atoms of elements that possess less than four valence electrons—if the required total number of four valence electrons per framework atom is provided via an electron transfer from guest atoms. Zintl phases of the group 14 elements (*Tt* = tetrel element) with alkali-metal (*A*), alkaline-earth-metal, or rare-earth-metal cations can possess polyanionic structure parts with exclusively four-connected atoms if electron poorer group 13 (*Tr* = triel element) or late-d-block metal (group 11 or group 12, *T*) atoms are included in the framework to build *Tr*−*Tt* or *T*−*Tt* polyanions, respectively.

Due to the need for new materials in the field of rechargeable batteries, there is a focus on phases that contain Li or Na ions as guests in the voids of a host network.[13,14] Furthermore, phases with open network structures that exhibit channels are of special interest, since they might serve as possible ion conductors. Among the ternary *A*−*Tr*−Sn and *A*−*T*−Sn phases with four-connected *Tr*−Sn or *T*−Sn networks, there are Li-containing phases that show diamond polytype like polyanionic networks (see e.g. refs 13, 15, and 16), while open clathrate structures are realized with K, Rb, and Cs (see e.g. refs 17−21). With intermediate-sized Na, there are some phases with different network structures of four-bonded atoms which have, other than the diamond and clathrate networks, no counterpart among group 14 element allotropes. The latter include the closely related Na−*Tr*−Sn compounds $NaGaSn_2$,[22] $NaInSn_2$,[23] and $NaGaSn_5$,[24] as well as the two isotypic $Na_5T_{2+x}Sn_{10-x}$ ($x \approx 0.5$) phases with *T* = Zn, Hg.[25] The three Na−*Tr*−Sn compounds show analogous *Tr*−Sn open framework structures with hexagonal helical channels that are filled with Na atoms. The $Na_5T_{2+x}Sn_{10-x}$ phases feature a new type of *T*−Sn network with realgar-like structural motifs.

Received: January 31, 2013
Published: May 21, 2013

dx.doi.org/10.1021/ja401043b | J. Am. Chem. Soc. 2013, 135, 10654−10663

Here we present Na_2ZnSn_5, another Sn-rich Na−Zn−Sn compound, and its relation to $Na_5Zn_{2+x}Sn_{10-x}$. Two modifications of the new Zintl compound have been characterized: *hP*-Na_2ZnSn_5 and *tI*-Na_2ZnSn_5. The Zn−Sn network of *hP*-Na_2ZnSn_5 is analogous to the *Tr*−Sn structure parts of $NaGaSn_2$,[22] $NaInSn_2$,[23] and $NaGaSn_5$.[24] *tI*-Na_2ZnSn_5, on the other hand, exhibits a closely related Zn−Sn four-connected open framework with a novel channel structure in which helical channels run in two perpendicular directions. The structural phase transition from *hP*-Na_2ZnSn_5 to *tI*-Na_2ZnSn_5 is accompanied by a Zn/Sn atom disorder−order transition. The topological description of the atom rearrangement bares facets of the fascinating structural possibilities for four-bonded networks.

EXPERIMENTAL SECTION

hP-Na_2ZnSn_5 and *tI*-Na_2ZnSn_5 were first obtained during exploratory syntheses in the Na−Zn−Sn system. After characterization of both phases by single-crystal XRD analyses, reaction conditions that allow the controlled synthesis of either one of the two modifications were determined in a series of experiments.

Differential Thermal Analysis. The reaction of the elements in the ratio Na:Zn:Sn = 2:1:5 was studied by means of a DTA experiment (for details see the Supporting Information, Text S-1 and Figure S-1). In the course of heating the mixture in the first cycle, the melting of Na and Sn and several other effects are visible. Upon cooling, a sharp exothermic effect at 368 °C (peak) indicates the crystallization of the product phase from the melt. As discussed below, the product after this first cycle is *hP*-Na_2ZnSn_5. During heating in the second cycle two distinct endothermic effects were recorded at 343 °C (onset) and at 384 °C (onset; peak at 392 °C). This shows that Na_2ZnSn_5 does not melt congruently. As will be discussed below, the effect observed at 343 °C (onset) corresponds to a transition that involves the (peritectic) decomposition of Na_2ZnSn_5 and the formation of $Na_5Zn_{2+x}Sn_{10-x}$ and elemental Sn. After the second effect (peak at 392 °C) the sample is all in the liquid state. The cooling curves of both cycles are virtually identical.

Syntheses. Niobium or tantalum ampules were loaded with the starting materials in an argon-filled glovebox. The ampules were sealed by arc welding under an argon atmosphere and then placed in silica tubes which were evacuated, sealed, and inserted in vertical resistance tube furnaces that were used to apply defined temperature programs to the samples. Samples were quenched by dropping the ampules into liquid nitrogen. The reaction products were characterized by means of powder XRD analyses.

In view of the results of the DTA experiment, four samples were treated as follows: mixtures of Na, Zn, and Sn in the ratio 2:1:5 (total sample loadings of approximately 1.5 g) were heated to 700 °C, cooled to 50 °C, and subsequently heated to target temperatures of approximately 300, 360, 380, and 450 °C, respectively (heating/cooling rates of 1 K/min). Each sample was hold for about 1 week at the respective target temperature and then quenched by dropping the ampule into liquid nitrogen.

***hP*-Na_2ZnSn_5.** *hP*-Na_2ZnSn_5 was obtained from the experiment with isothermal dwelling at 450 °C. In this case, the quenching of the sample represents the (very) fast cooling of a melt of composition Na:Zn:Sn = 2:1:5. Further, experiments with the same temperature program as used for the DTA measurement (heating/cooling rate of 1 K/min and an upper target temperature of 700 °C) confirmed that these reaction conditions also reproducibly lead to the formation of *hP*-Na_2ZnSn_5, regardless of whether one or more heating/cooling cycles were applied.

***tI*-Na_2ZnSn_5 and Phase Transition from *hP*-Na_2ZnSn_5 to *tI*-Na_2ZnSn_5.** The product of the experiment with isothermal dwelling at 300 °C was *tI*-Na_2ZnSn_5. The reaction conditions involve tempering of *hP*-Na_2ZnSn_5 at a temperature below the endothermic effect that is visible at higher temperature in the second cycle of the DTA experiment (onset 343 °C). These findings were confirmed by an experiment starting with a sample of *hP*-Na_2ZnSn_5 that was characterized by powder XRD analysis prior to being pressed to a pellet, heated to approximately 300 °C, annealed at this temperature, and finally quenched. Notably, this polymorphic phase transition from *hP*-Na_2ZnSn_5 to *tI*-Na_2ZnSn_5 was not detected in our DTA experiments. *tI*-Na_2ZnSn_5 was also obtained by heating a stoichiometric mixture of the elements to 450 °C followed by very slow cooling at a rate of 0.1 K/min.

$Na_5Zn_{2+x}Sn_{10-x}$. Applying dwelling temperatures of approximately 360 and 380 °C (between the two endothermic effects observed in the DTA experiment; see the Supporting Information, Figure S-1) results in the formation of $Na_5Zn_{2+x}Sn_{10-x}$ and *β*-Sn. Thus, the thermal effect that was observed in the second cycle of the DTA experiment at 343 °C (onset) is attributed to the (peritectic) decomposition of Na_2ZnSn_5. This result was confirmed by heating a pressed pellet of *hP*-Na_2ZnSn_5 to approximately 360 °C, annealing the sample at this temperature for 1 week, and finally quenching it.

Powder X-ray Diffraction, Including Temperature-Dependent Experiments. For powder XRD measurements, samples of the reaction products were finely ground, optionally diluted with diamond powder, and sealed in glass capillaries (silica for high-temperature measurements) in an argon-filled glovebox. Powder XRD data were collected with a STOE STADI P powder diffractometer equipped with an imaging plate and a linear position sensitive detector (IP-PSD and L-PSD) using Cu Kα_1 radiation (λ = 1.54060 Å, curved Ge(111) monochromator). For temperature-dependent (high-temperature) powder XRD experiments a capillary furnace high-temperature attachment, version 0.65.3, was employed and data were collected with the imaging plate detector (IP-PSD). The STOE WINXPOW program package[26] was used for data evaluation. The lattice parameters of *hP*-Na_2ZnSn_5 and *tI*-Na_2ZnSn_5 (see e.g. Table 1) were obtained by Rietveld refinements of data sets collected at room temperature with the L-PSD. The FULLPROF SUITE software[27−29] was employed for the Rietveld analyses.

hP-Na_2ZnSn_5 was heated and XRD measurements with the temperature held constant during data collection were carried out at steps of 25 K from 25 to 150 °C and at steps of 10 K from 150 to 340 °C. The phase transition from *hP*-Na_2ZnSn_5 to *tI*-Na_2ZnSn_5 was observed at approximately 250 °C (Figure 4).

tI-Na_2ZnSn_5 was heated and XRD measurements with the temperature held constant during data collection were taken at 25, 150, 200, 250, and 280 °C and at steps of 5 K in the range from 290 to 380 °C. *tI*-Na_2ZnSn_5 was observed to be stable up to about 350 °C (Supporting Information, Figure S-2).

Single-Crystal X-ray Diffraction and Crystal Structure Determinations. Suitable single crystals of *hP*-Na_2ZnSn_5 and *tI*-Na_2ZnSn_5 were selected in an argon-filled glovebox equipped with a microscope. The crystals were fixed on glass fibers with perfluoropolyalkyl ether. For *hP*-Na_2ZnSn_5, single-crystal XRD data were collected at 110 K (OXFORD Instruments Cryojet cooling system, nitrogen jet) with a BRUKER APEX II diffractometer system (KAPPA goniometer, APEX II CCD detector) using Mo Kα radiation (λ = 0.71073 Å, graphite monochromator, rotating anode source). ω and φ scans (18 runs, total of 3268 images) were performed with an exposure time of 15 s and increments of 1° per frame; the detector distance was set to 35 mm. The BRUKER SAINT software was used for data processing, including an absorption correction with SADABS. For *tI*-Na_2ZnSn_5, single-crystal XRD data were collected at 150 K (Oxford Instruments Cryojet cooling system, nitrogen jet) with an OXFORD Xcalibur3 diffractometer with a Sapphire 3 CCD detector using Mo Kα radiation (λ = 0.71073 Å, graphite monochromator). With an exposure time of 20 s, a frame width of 1°, and a detector distance of 50 mm, a total of 776 frames were collected in four ω scans (ω = −41 to +63°, κ = −79°, θ = 30°, φ = 0, 90, 180, 270°) and one φ scan (φ = 0−360°, θ = 30°, ω = 0°, κ = 0°). The OXFORD CrysAlis RED software[30] was used for data processing. A numerical absorption correction was applied with the STOE X-RED[31]/X-SHAPE[32] software. For both *hP*-Na_2ZnSn_5 and *tI*-Na_2ZnSn_5, XPREP[33] was used for space group determination and data merging (identical indices only) and the programs XS[34,35] and XL[35,36] were used for structure solution (direct

dx.doi.org/10.1021/ja401043b | J. Am. Chem. Soc. 2013, 135, 10654−10663

Table 1. Selected Crystallographic, Data Collection, and Refinement Data for *hP*-Na_2ZnSn_5 and *tI*-Na_2ZnSn_5

formula[a] and Bravais lattice type	*hP*-Na_2ZnSn_5	*tI*-Na_2ZnSn_5
formula wt, M/g mol^{-1}	704.80	704.80
space group	$P6_122$ (No. 178)	$I\bar{4}2d$ (No. 122)
Z	1	4
unit cell params[b]		
a/Å	6.451(1)	6.336(1)
c/Å	6.237(1)	22.382(1)
unit cell volume, V/Å^3	224.78(6)	898.5(2)
calcd density, ρ_{calcd}/g cm^{-3}	5.207	5.210
abs coeff (Mo Kα), μ/mm^{-1}	16.30	16.31
F(000)	302	1208
cryst color, shape	silvery, block	silvery, block
temp for single-crystal data collection, T/K	110	150
wavelength (Mo Kα), λ/Å	0.71073	0.71073
diffractometer	BRUKER APEX II	OXFORD Xcalibur 3
θ range/deg	3.65−30.42	3.34−26.00
limiting indices	$-9 \le h \le 9$; $-8 \le k \le 7$; $-8 \le l \le 8$	$-7 \le h \le 7$; $-7 \le k \le 7$; $-27 \le l \le 27$
no. of measd/unique rflns	2321/230	2919/449
completeness/%	100	100
R_σ, R_{int}	0.014, 0.032	0.027, 0.045
refinement method	full-matrix least squares on F^2, with XL	
no. of data/restraints/params	230/2/14	449/1/24
extinction coeff	0.015(2)	
Flack param	0.2(5)	0.03(15)
largest diff peak and hole/e Å^{-3}	+0.858 and −0.528	+1.963 and −0.865
goodness of fit on F^2	1.336	1.057
R_1, wR_2 ($I > 2\sigma(I)$)	0.016, 0.038	0.032, 0.077
R_1, wR_2 (all data)	0.016, 0.038	0.036, 0.078

[a]See the Experimental Section for details on the refinement with partially occupied Na sites and also the Zn/Sn mixed occupancy in the case of *hP*-Na_2ZnSn_5. [b]Unit cell parameters determined by Rietveld analyses of powder XRD data obtained at room temperature.

methods) and structure refinement (full-matrix least squares on F_o^2), respectively. Atomic coordinates were standardized with the program STRUCTURE TIDY[37] implemented in PLATON.[38] Atomic coordinates and equivalent isotropic displacement parameters are given in Table 2, and anisotropic displacement parameters are given in Table 3.

The structure of *tI*-Na_2ZnSn_5 was solved in space group $I\bar{4}2d$ (No. 122). A Flack parameter of 0.03(15) was calculated in the final refinement. The structure model for *tI*-Na_2ZnSn_5 shows full ordering of Zn and Sn on three sites (Zn on 4*a*, Sn1 on 16*e*, and Sn2 on 4*b*) and involves a partially occupied Na position (on 16*e*). The freely refined value for the occupancy factor of the Na site is 0.47(2), in agreement with the value of $^1/_2$ that results in the overall composition Na:Zn:Sn = 2:1:5. In the final refinement steps the parameter was fixed to 0.5.

The structure of *hP*-Na_2ZnSn_5 was solved in space group $P6_122$ (No. 178). In the final refinement a Flack parameter of 0.2(5) was calculated. Thus, the absolute structure or the volume fraction of an inversion twin could not be determined reliably, and the structure could alternatively be described in the enantiomorphic space group $P6_522$ (No. 179). The structure model provides only one site (6*b*) for the Zn and Sn atoms, which has consequently mixed occupancy. Since the phase was found to represent a modification of Na_2ZnSn_5 (see below), the Zn:Sn ratio was fixed to 1:5 ($^1/_6$:$^5/_6$) in the refinement. With only one Zn/Sn mixed-occupancy site for the atoms of the anionic substructure, and one partially occupied site (6*b*) for the Na atoms, the Zn:Sn ratio could not be determined reliably only from the single-crystal XRD data for the hexagonal phase. Free refinement of the occupancy factor for the Na position led to a value of 0.35(2). Since single crystals (drilling) of *tI*-Na_2ZnSn_5 form from single crystals of *hP*-Na_2ZnSn_5 (see below) and the composition of the latter has been reliably determined from XRD, all occupation parameters were fixed in the final refinement steps, meeting the overall composition of Na_2ZnSn_5.

EDX Measurements. EDX analyses of single crystals of *hP*-Na_2ZnSn_5 and *tI*-Na_2ZnSn_5 (unit cell determined by single-crystal XRD prior to EDX analysis) were carried out using a JEOL 5900LV scanning electron microscope equipped with an OXFORD Instruments INCA energy dispersive X-ray microanalysis system. The qualitative analyses showed the presence of Na, Zn, and Sn and the absence of other elements heavier than Na.

Temperature-Dependent Single-Crystal XRD Measurements. With a STOE IPDS 2T imaging plate diffractometer using Mo Kα radiation (λ = 0.71073 Å, graphite monochromator, rotating anode source) that was equipped with a HEATSTREAM high-temperature attachment (heating medium N_2, vertical gas flow), temperature-dependent single-crystal XRD measurements were performed at higher temperatures. Suitable single crystals of *hP*-Na_2ZnSn_5 were selected in an argon-filled glovebox equipped with a microscope. The crystals were sealed in glass capillaries, in which they were fixed with glass fibers (not using any sort of glue). During heating of crystals of *hP*-Na_2ZnSn_5 on the diffractometer, a transition could be observed. The analysis of a data set collected after the phase transition led to the conclusion that a drilling of *tI*-Na_2ZnSn_5 had formed. (Details on the data collection and refinement results are given in the Supporting Information, Text S-2 and Tables S-1, S-2, and S-3.) Measurements with a crystal that had undergone the transition and was subsequently cooled to 20 °C again confirmed that the transition is not reversible.

Electronic Structure Calculations. DFT calculations were carried out with the Stuttgart TB-LMTO-ASA program,[39] employing the tight-binding (TB) version of the linear muffin-tin orbital (LMTO) method in the atomic sphere approximation (ASA). The

Table 2. Atomic Coordinates and Equivalent Isotropic Displacement Parameters for *hP*-Na_2ZnSn_5 and *tI*-Na_2ZnSn_5[a]

atom	Wyckoff	occ	x	y	z	U_{eq}/Å^2
			hP-Na_2ZnSn_5			
Zn/Sn	6*b*	Zn:Sn = $^1/_6$:$^5/_6$[b]	0.7643(1)	0.5286(1)	$^1/_4$	0.016(1)
Na	6*b*	$^1/_3$[b]	0.103(1)	0.205(2)	$^1/_4$	0.052(3)
			tI-Na_2ZnSn_5			
Sn1	16*e*		0.1572(1)	0.1679(1)	0.3154(1)	0.018(1)
Sn2	4*b*		0	0	$^1/_2$	0.018(1)
Zn	4*a*		0	0	0	0.019(2)
Na	16*e*	$^1/_2$[b]	0.150(2)	0.198(2)	0.145(1)	0.038(3)

[a]U_{eq} is defined as one-third of the trace of the orthogonalized U_{ij} tensor. [b]Occupancy factors fixed in final refinement steps.

dx.doi.org/10.1021/ja401043b | J. Am. Chem. Soc. 2013, 135, 10654−10663

Table 3. Anisotropic Displacement Parameters (U_{ij}/Å^2) for *hP*-Na_2ZnSn_5 and *tI*-Na_2ZnSn_5

atom	U_{11}	U_{22}	U_{33}	U_{23}	U_{13}	U_{12}
			hP-Na_2ZnSn_5			
Zn/Sn	0.013(1)	0.015(1)	0.020(1)	0	−0.004(1)	0.007(1)
Na	0.056(5)	0.028(4)	0.062(6)	0	−0.053(5)	0.014(2)
			tI-Na_2ZnSn_5			
Sn1	0.020(1)	0.022(1)	0.013(1)	0.003(1)	0.000(1)	−0.001(1)
Sn2	0.022(1)	0.022(1)	0.009(1)	0	0	0
Zn	0.022(1)	0.022(1)	0.013(1)	0	0	0
Na	0.029(5)	0.033(7)	0.050(8)	−0.016(5)	−0.008(5)	0.007(6)

Barth−Hedin local exchange correlation potential[40] was used. Radii of the atomic spheres and interstitial empty spheres were determined by the procedures implemented in the TB-LMTO-ASA programs. The *k*-space integration was performed by the tetrahedron method.[41] Na 3s/(3p)/(3d), Zn 4s/4p/3d, and Sn 5s/5p/(5d)/(4f) states were included in the calculations (downfolded in parentheses). VESTA[42] was used to prepare graphical representations of the electron localization function (ELF).

The calculations were performed for ordered model structures that were deduced from a description of a pathway for the structural transition from *hP*-Na_2ZnSn_5 to *tI*-Na_2ZnSn_5 (see Figure 5 and the Supporting Information Figure S-3 and Tables S-4 and S-5). The structural parameters of the model structures are based on the experimentally determined unit cell parameters and atomic coordinates. Totals of 1040 and 1056 irreducible *k*-points were used for the calculations for the models for *tI*-Na_2ZnSn_5 and *hP*-Na_2ZnSn_5, respectively.

For *tI*-Na_2ZnSn_5, the model structure ($P2_1$ (No. 4); a = 6.336 Å, b = 22.382 Å, c = 6.336 Å) with ordered Na positions is taken for a valid description. Concerning the employed model structure for *hP*-Na_2ZnSn_5 ($P2_1$ (No. 4); a = 22.347 Å, b = 6.237 Å, c = 6.451 Å) with ordered Zn and Sn atom positions and ordered Na positions, it must be noted that it features helical chains (see text for structure description) of different types which contain two, one, or no Zn atoms per turn of the helix. While this is needed to depict the structural relations between the two Na_2ZnSn_5 modifications as shown in Figure 5, it is obviously not designed to best account for a statistical distribution of Zn atoms on the network positions. Further, the model involves e.g. the Zn/Sn−Zn/Sn site distances, instead of unequal Zn−Sn and Sn−Sn distances (as would be expected for an optimized ordered structure). For this reason, the calculated (P)DOS for this model is only included in the Supporting Information (Figure S-4) for the sake of completeness. In the Supporting Information also the results of the ELF analysis for both model structures are presented (Figures S-5 and S-6 and Text S-3).

RESULTS AND DISCUSSION

While the Na:Zn:Sn ratio can be deduced from single-crystal XRD data for *tI*-Na_2ZnSn_5, the composition of *hP*-Na_2ZnSn_5 could not be determined reliably by this means, since the anionic structure part is formed by only one crystallographic site, which has mixed occupancy with Zn and Sn atoms. That the two phases represent two modifications of Na_2ZnSn_5 is shown by controlled syntheses of either *hP*-Na_2ZnSn_5 or *tI*-Na_2ZnSn_5 by reactions of mixtures of the elements in the ratio Na:Zn:Sn = 2:1:5, as well as by in situ investigations of the phase transformation from *hP*-Na_2ZnSn_5 to *tI*-Na_2ZnSn_5 by means of temperature-dependent powder and single-crystal XRD measurements.

Description of the Crystal Structures. *hP*-Na_2ZnSn_5 and *tI*-Na_2ZnSn_5 show open network structures of four-bonded Zn and Sn atoms with hexagonal helical channels in which the Na atoms are situated with disorder.

The structure of *hP*-Na_2ZnSn_5 (Figure 1) is described with hexagonal symmetry in the space group $P6_122$ with lattice

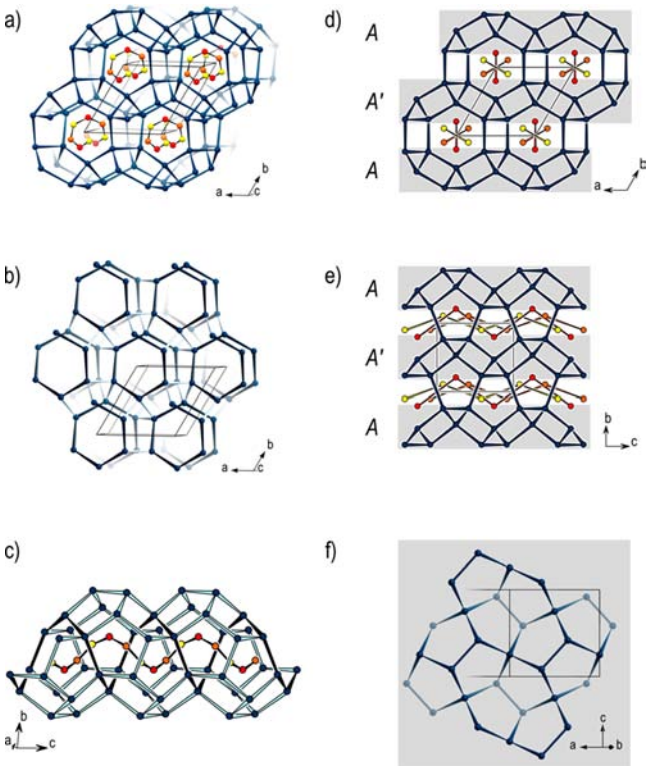

Figure 1. Representation of the structure of *hP*-Na_2ZnSn_5: (a) four-connected Zn−Sn framework with helical channels filled with Na atoms; (b) Zn−Sn framework structure, with hexagonal helical chains running along the *c* direction emphasized; (c) Na positions located in one of the hexagonal channels; (d) parallel projection in the direction of the hexagonal channels, with emphasis on one of the three equivalent sets (see Figure 6) of puckered layers of Zn and Sn atoms (gray background); (e) side view of the hexagonal helical channels and Na positions, with puckered layers of Zn and Sn atoms highlighted (gray background); (f) top view of one of the puckered layers of five-membered rings (highlighted in (d) and (e)) as also occurs in $NaSn_5$.[43] Zn/Sn mixed-occupancy positions are represented in dark teal. The occupancy factor for the Na site is $^1/_3$, and three ordered models for the Na positions are shown in red, orange, and yellow.

parameters a = 6.451(1) Å and c = 6.237(1) Å. In Figure 1b, the Zn−Sn network of *hP*-Na_2ZnSn_5 is depicted, emphasizing hexagonal helical chains running parallel to the *c* direction. These chains are aligned in the style of hexagonal rod packing and interconnected so that channels with partition walls made of five-membered rings result (Figure 1c). The description in space group $P6_122$ involves right-handed helices, while the

dx.doi.org/10.1021/ja401043b | J. Am. Chem. Soc. 2013, 135, 10654−10663

corresponding structure with left-handed helices is associated with the enantiomorphic space group $P6_522$. The Zn−Sn network structure is realized with only one crystallographic site (6*b*), which has consequently mixed occupancy with Zn and Sn atoms. Each network atom exclusively belongs to one helical chain and is involved in two intrachain bonds (d(Zn/Sn−Zn/Sn) = 2.831(1) Å) and two bonds to atoms of two adjacent helical chains (d(Zn/Sn−Zn/Sn) = 2.810(1) Å). There is also only one, partially occupied, Na site (6*b*), which generates hexagonal helical chains of Na atom positions inside the channels (Figure 1c). The occupancy factor for the Na site is $^1/_3$ (cf. the Experimental Section), and ordered models with every third Na position of a chain occupied involve reasonable Na−Na distances of 3.87 Å (see Figure 1d,e). Distances (<4 Å) between Na sites and Zn/Sn positions range from 3.09 to 3.78 Å.

An alternative description of the Zn−Sn structure part highlights puckered layers of five-membered rings (Figure 1d−f) as also occur in $NaSn_5$.[43] A set of layers extending parallel to *ac* is marked in Figure 1d,e. The layers are stacked and interconnected so that hexagonal helical channels result. Taking the stacking direction perpendicular to *ac*, the stacking sequence is *AA′* (Figures 1d,e). Of course, due to the 3-fold symmetry axes parallel to the *c* direction, there are three equivalent layer sets (see Figure 6).

The structure of *tI*-Na_2ZnSn_5 (Figure 2), which is described in space group $I\bar{4}2d$ (No. 122) with lattice parameters a = 6.336(1) Å and c = 22.382(1) Å, is closely related to that of *hP*-Na_2ZnSn_5. In the case of *tI*-Na_2ZnSn_5, Zn and Sn atoms are fully ordered on three sites, and puckered layers of five-membered rings extend parallel to *ab* with the stacking sequence *AA′A″A‴* along the *c* direction (Figure 2d). As a consequence of this different stacking sequence, channels are aligned in layers of parallel channels that run alternately along *a* and *b*. Helical Zn−Sn chains running in perpendicular directions share Zn atoms (on the 4*a* site) at nodal points, as shown in Figure 2b. Sn1 atoms (on 16*e*) are part of one helical chain; Sn2 atoms (on 4*b*) do not belong to any helical chain. The helices along *a* are left-handed, and those along *b* are right-handed (Figure 2b). Within one helical chain, the Zn−Sn1 and Sn1−Sn1 distances are 2.750(1) and 2.914(2) Å, respectively. The Sn1−Sn1 distances between Sn1 atoms of neighboring helical chains are 2.915(2) Å. The shortest Sn−Sn distances of 2.827(1) Å are found for the Sn1−Sn2 contacts.

Na atoms fill the channels of the Zn−Sn framework (Figure 2a,c,d). The occupancy factor of the Na site (16*e*) is $^1/_2$, resulting in the composition Na:Zn:Sn = 2:1:5. An ordered model in which every second Na position along the line is occupied involves reasonable Na−Na distances of 3.81 Å. The Na−Zn and Na−Sn distances <4 Å are in the range from 3.09 to 3.82 Å.

Electronic Structure of *tI*-Na_2ZnSn_5. All bond lengths reveal covalent Sn−Sn and Zn−Sn bonds. Thus, formally including (4b-Sn^0) and (4b-Zn^{2-}) framework atoms (4b: four-bonded), both Na_2ZnSn_5 modifications are Zintl phases with polyanionic Zn−Sn networks that match the 8 − N rule. The calculated (TB-LMTO-ASA) band structure for *tI*-Na_2ZnSn_5, in which Zn and Sn atoms occur ordered, shows a band gap of approximately 0.5 eV at the Fermi level, as expected for a Zintl phase. For the calculation a model with ordered Na atoms has been used (see Table S-5 in the Supporting Information and also Figure 5c,f).

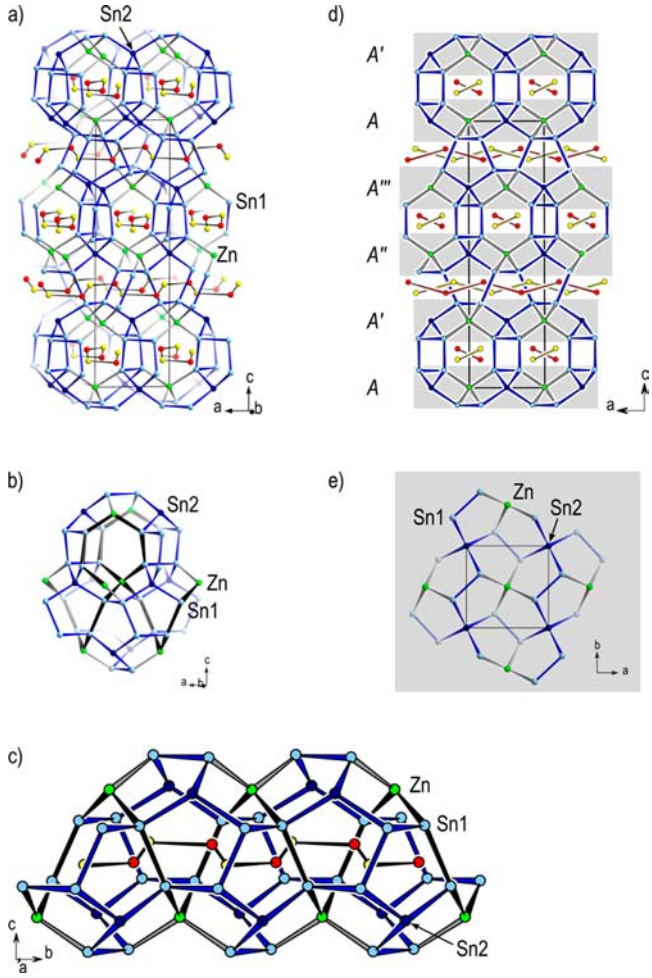

Figure 2. Representation of the structure of *tI*-Na_2ZnSn_5: (a) four-connected Zn−Sn framework with helical channels filled with Na atoms; (b) (distorted) hexagonal helical chains and channels of Zn and Sn atoms in the *a* and *b* directions; (c) Na positions located in one of the channels; (d) projection along *b*, with puckered layers of Zn and Sn atoms highlighted (gray background); (e) top view of a puckered layer of five-membered rings highlighted in (d). Sn and Zn atoms are shown in blue and green, respectively. The occupancy factor for the Na site is $^1/_2$, and two ordered models for the Na positions are shown in red and yellow.

Total DOS (density of states) plots as well as atom type and orbital type resolved partial density of states (PDOS) plots for *tI*-Na_2ZnSn_5 are shown in Figure 3. Sn p and Zn p states prevail just below the Fermi level. The PDOS analysis supports the description of the Zn−Sn network of Na_2ZnSn_5 as an s−p-bonded framework, Zn acts as a "pseudo main group metal". The Zn d states can be regarded as "pseudo core states", giving rise to the main DOS peak at approximately −8 eV. Note that Na states also make important contributions to the total DOS. The (P)DOS for the ordered model structure for *hP*-Na_2ZnSn_5 is shown in the Supporting Information (Figure S-4), as well as analyses of the electron localization function (ELF) for the model structures for both *tI*-Na_2ZnSn_5 and *hP*-Na_2ZnSn_5 (Figures S-5 and S-6, Text S-3).

Controlled Syntheses of the Two Modifications of Na_2ZnSn_5 and the Polymorphic Phase Transition. *hP*-Na_2ZnSn_5 forms if a melt arising from heating a stoichiometric mixture of the elements is quenched or cooled at a rate of 1 K/min. In contrast, *tI*-Na_2ZnSn_5 is obtained if a

dx.doi.org/10.1021/ja401043b | J. Am. Chem. Soc. 2013, 135, 10654−10663

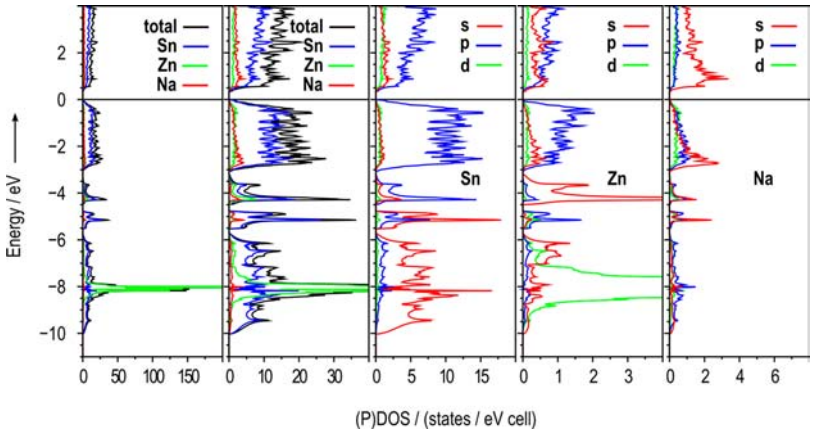

Figure 3. Total and partial density of states curves for *tI*-Na_2ZnSn_5 (model with ordered Na sites). The Fermi level (E_F) is at 0 eV. Notice that different scales are used for the representations of the PDOS curves for Sn, Zn, and Na, taking into account the composition of Na_2ZnSn_5.

very slow cooling rate (0.1 K/min) is used. These findings indicate that *hP*-Na_2ZnSn_5 is kinetically favored, while *tI*-Na_2ZnSn_5 is the thermodynamically stable modification at standard conditions. This interpretation is in accord with the observation that *tI*-Na_2ZnSn_5 forms if a sample of *hP*-Na_2ZnSn_5 is annealed at 300 °C, a temperature below the first thermal effect that is observed in the DTA experiment when heating *hP*-Na_2ZnSn_5 (see the Supporting Information). Though the polymorphic phase transition was not observed in the DTA experiment, two exothermic effects are apparent in the heating curve, revealing that Na_2ZnSn_5 does not melt congruently. A first effect at 343 °C (onset) is attributed to the (peritectic) decomposition of Na_2ZnSn_5 and the formation of $Na_5Zn_{2+x}Sn_{10-x}$ with a lower Sn content. At temperatures above the second effect (onset 384 °C) the sample is all in the liquid state.

The results of the thermal analysis have been confirmed by temperature-dependent powder XRD experiments in the temperature range from 25 to 380 °C. When *hP*-Na_2ZnSn_5 is heated, only the reflections of *hP*-Na_2ZnSn_5 occur up to a temperature of 220 °C (Figure 4). At 240 °C both *hP*-Na_2ZnSn_5 and *tI*-Na_2ZnSn_5 are present, and in the temperature range from 260 to 340 °C only the reflections of *tI*-Na_2ZnSn_5 were observed. During heating of a single crystal of *hP*-Na_2ZnSn_5, the transition was observed as well, with

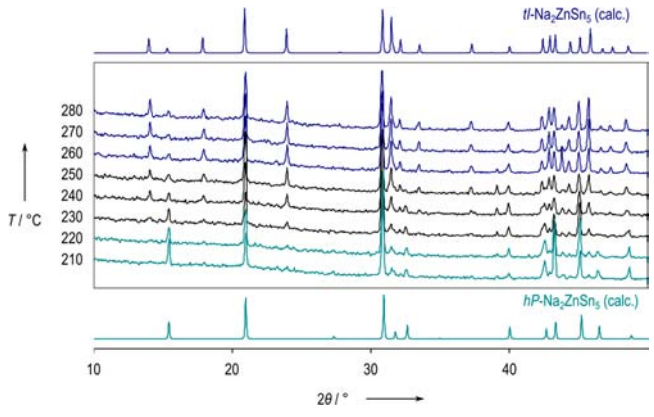

Figure 4. Powder XRD patterns obtained from temperature-dependent measurements (heating) of a sample of *hP*-Na_2ZnSn_5. The phase transition from *hP*-Na_2ZnSn_5 to *tI*-Na_2ZnSn_5 is observed at about 250 °C.

formation of a drilling of *tI*-Na_2ZnSn_5. Cooling a crystal that had undergone the transition back to room temperature confirmed that the transition is not reversible. Heating of *tI*-Na_2ZnSn_5 shows, in accordance with the results of the DTA experiment (effect at 343 °C), that the phase is stable up to about 350 °C. The powder XRD patterns also show the decomposition of the compound at higher temperatures (see the Supporting Information, Figure S-2). As described above, tempering experiments in sealed metal ampules showed that the decomposition of Na_2ZnSn_5 yields $Na_5Zn_{2+x}Sn_{10-x}$. With the in situ high-temperature powder XRD experiments, the formation of $Na_5Zn_{2+x}Sn_{10-x}$ could, however, not be observed directly.

The experimental results establish the two title phases as modifications of the ternary compound Na_2ZnSn_5. *tI*-Na_2ZnSn_5 is the thermodynamically stable polymorph, while *hP*-Na_2ZnSn_5 is a metastable phase under standard conditions.

Topological Transformation between the *hP*-Na_2ZnSn_5 and *tI*-Na_2ZnSn_5 Structures. A path for the interconversion between the structures of the two Na_2ZnSn_5 modifications is depicted in Figure 5. In addition to the rearrangement of the Zn−Sn network and the Na atoms, the transformation also involves an ordering of Zn and Sn atom sites in the framework. Therefore, a suitable superstructure for *hP*-Na_2ZnSn_5 with fully ordered atom sites ($P2_1$; a = 22.347 Å, b = 6.237 Å, c = 6.451 Å) is set up (Figure 5a). The illustration further uses suitable models with ordered Na atoms for both *hP*- and *tI*-Na_2ZnSn_5. All structural parameters for these models are given in the Supporting Information (Tables S-4 and S-5). Figure S-3 in the Supporting Information shows the group−subgroup relations between the experimental and ordered structure models. The link between the two network structures is highlighted by the dashed blue lines in Figure 5, indicating formal Sn−Sn bond scission (Figure 5a,d,g) and bond formation (Figure 5b,e,h). The (re)orientation of the chains of Na atoms is indicated by (dashed) red lines. Two out of four puckered layers of pentagons and their neighboring Na atoms are affected by these changes (Figure 5d−f); one layer is shown in the top view in Figure 5g−i. This description of the structural transition nicely illustrates the close relationship between the two structures. But of course, the actual mechanism of the phase transition on the atomic scale is not known, and no conclusions concerning the classification of the phase transition should be drawn.

dx.doi.org/10.1021/ja401043b | J. Am. Chem. Soc. 2013, 135, 10654−10663

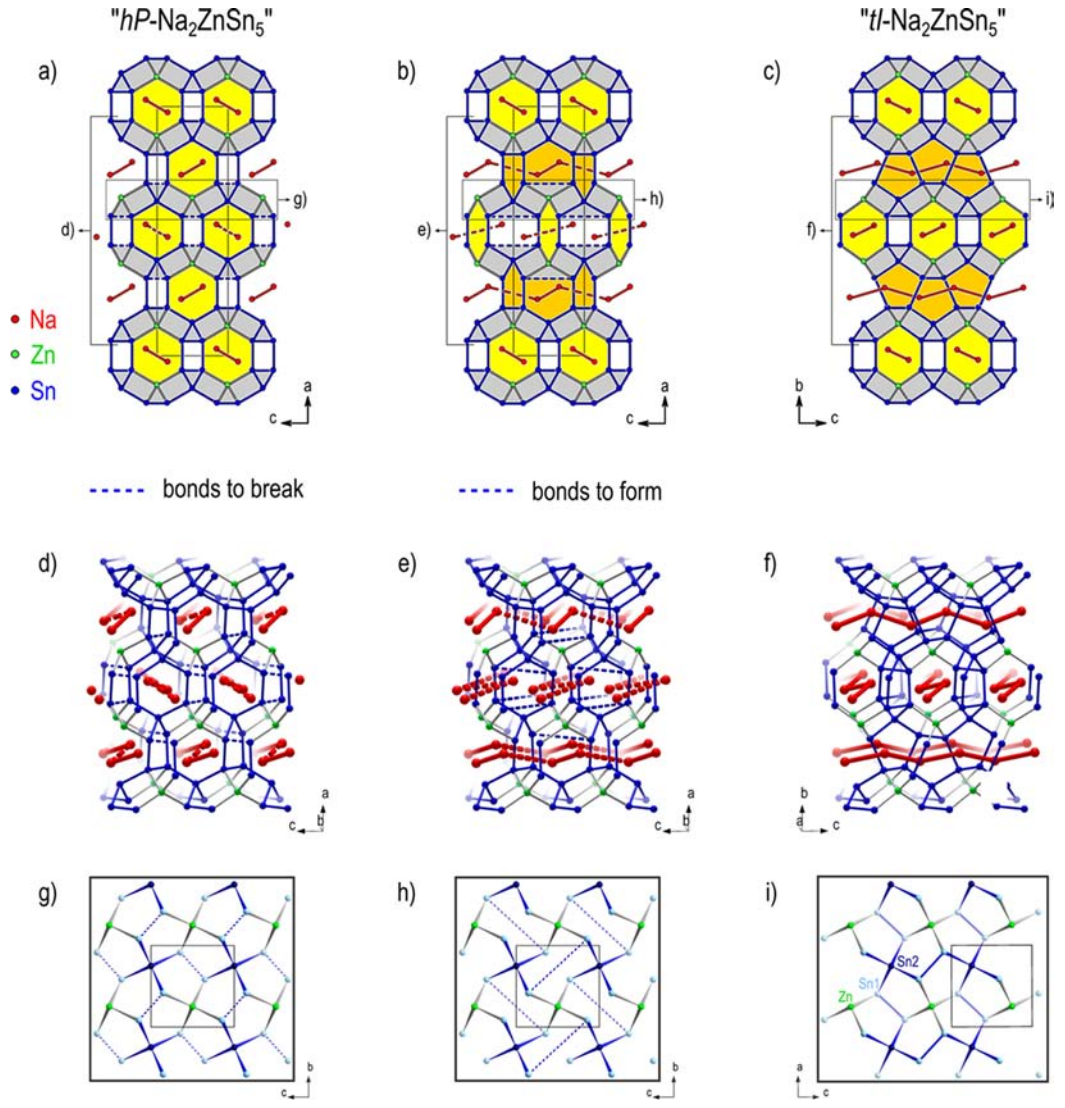

Figure 5. Pathway for the structural transition from *hP*-Na_2ZnSn_5 to *tI*-Na_2ZnSn_5 (left to right): (a–c) overview in parallel projection; (d–f) focus on the structural part where bond scission and bond formation take place; (g–i) illustration of the changes in a puckered layer of five-membered rings (top view). In parts a, b, d, e, g, and h atom positions of a fully ordered superstructure model for *hP*-Na_2ZnSn_5 are shown. In parts c, f, and i the model for *tI*-Na_2ZnSn_5 with ordered Na sites is depicted. Dashed blue lines in parts a, d, and g indicate bond scission in the network, and dashed blue lines in parts b, e, and h indicate bond formation during the transition of the network structure. Dashed red lines between Na atoms indicate the rearrangement of the Na atoms. Na, Zn, and Sn atoms are represented as red, green and (light or dark) blue spheres, respectively. For further explanations, see the text.

However, due to the symmetry of the crystal structure of *hP*-Na_2ZnSn_5, the formal transformation described above can alternatively occur for one of the layer sets oriented in 120° directions (Figure 6), and the three equivalent possibilities nicely correspond to the observation that heating a single crystal of *hP*-Na_2ZnSn_5 leads to the formation of a drilling of *tI*-Na_2ZnSn_5.

Relationship between the Four-Bonded Networks of Na_2ZnSn_5 and $Na_5Zn_{2+x}Sn_{10-x}$. The observation that the decomposition of Na_2ZnSn_5 yields $Na_5Zn_{2+x}Sn_{10-x}$ calls for a further analysis of the structural relations between the different networks with exclusively four-connected atoms that form the Zn–Sn parts of these phases. The phases differ in composition, but still, the analysis reveals a close relationship of the network structures—furthermore, it opens perspectives for a whole series of new four-connected networks. Actually, the layers that occur as building blocks in the network structures of the two Na_2ZnSn_5 modifications and $Na_5Zn_{2+x}Sn_{10-x}$ can be traced back to the basic cubic diamond structure of α-Sn, as illustrated in Figure 7. Figure 7a,b shows how layers of four- and two-connected atoms can be cut out of the α-Sn structure. In the case of tin's lighter homologue Ge such two-dimensional structural parts actually occur in the tetragonal high-pressure modification of LiGe.[44]

There are various ways to distort such a two-dimensional section of the cubic diamond structure (1) (Figure 7) by bond formation leading to layers with four- and three-connected atoms. Bond formation in analogy to the basket-weave rectangular tiling (2a), with relocation of the atoms to reach approximately equal bond lengths, yields a layer structure that corresponds to the Cairo-type (pentagonal) tiling (2b), as is found for the two modifications of Na_2ZnSn_5 and $NaSn_5$[43] (Figure 7d, left side). For a defined domain of the layer, there are two possible orientations for a basket-weave pattern (Figure

dx.doi.org/10.1021/ja401043b | J. Am. Chem. Soc. 2013, 135, 10654–10663

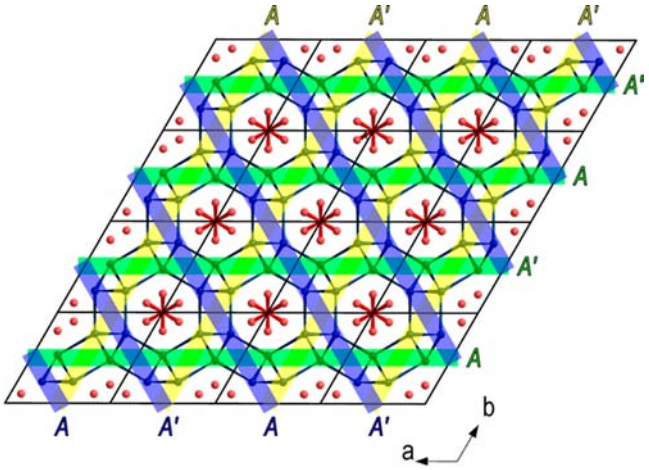

Figure 6. Stacking of puckered layers of five-membered rings in the structure of *hP*-Na_2ZnSn_5. The three possible choices for the stacking direction are shown. The layers correspond to those highlighted with a gray background in Figures 1 and 5a.

8a). The interchange between these two patterns corresponds to the structural changes during the interconversion between the network structures of *hP*-Na_2ZnSn_5 and *tI*-Na_2ZnSn_5, as shown in Figure 5. The rearrangement of the five-membered rings resembles the diamond−square−diamond mechanism which is used to describe the rearrangement of triangles (Figure 8b) in transformations of deltahedral cages of carboranes.[45,46] A layer with realgar-like structural motifs as occurs in $Na_5Zn_{2+x}Sn_{10-x}$[25] can be obtained by a distortion of (1) with bond formation according to (3a) and (3b) (Figure 7).

Figure 7 also shows the relations between the dimensions of the repeating units of the different layer types, as well as the unit cell dimensions of α-Sn (cubic diamond structure), *hP*- and *tI*-Na_2ZnSn_5, and $Na_5Zn_{2+x}Sn_{10-x}$. The actual structural parameters for the compounds are given in Table 4 and fit well with the scheme. The lengths of the unit cell axes parallel to the layers of α-Sn, *hP*-, and *tI*-Na_2ZnSn_5 differ only slightly and also compare well to those of $Na_5Zn_{2+x}Sn_{10-x}$ which are approximately doubled. Table 4 also gives the lattice parameters along the stacking directions and the corresponding number of layers. This also reveals the close relationship between the networks built up of stacked and interconnected layers.

***hP*-Na_2ZnSn_5 and Related Na−*Tr*−Sn (*Tr* = Ga, In) Compounds.** The Zn−Sn framework structure of *hP*-Na_2ZnSn_5 is analogous to the *Tr*−Sn (*Tr* = Ga, In) structure parts of $NaInSn_2$,[23] $NaGaSn_2$,[22] and $NaGaSn_5$.[24] Selected structural data for these phases, which are all electron-precise Zintl compounds (with ratios of Na:Zn = 2:1 or Na:*Tr* = 1:1), are given in Table 5. For all of them, exclusively mixed-occupancy sites have been reported for the network atoms, and for all but $NaInSn_2$ also a disorder of the Na atoms has been described (with split and/or partially occupied Na sites). The relations between the assigned space groups are given in the Supporting Information (Figure S-7). The observed phase transformation of *hP*-Na_2ZnSn_5 to *tI*-Na_2ZnSn_5 unequivocally reveals also the composition of the phase with Zn/Sn disorder and shows the validity of the Zintl concept for this structure. The findings on Na_2ZnSn_5 suggest that atom ordering and polymorphic transitions may also occur for the other phases of this structure family.

Four-Bonded Networks: Outlook. Recently, theoretical studies considered an (empty) framework structure with helical channels in one direction[47] that is analogous to the framework

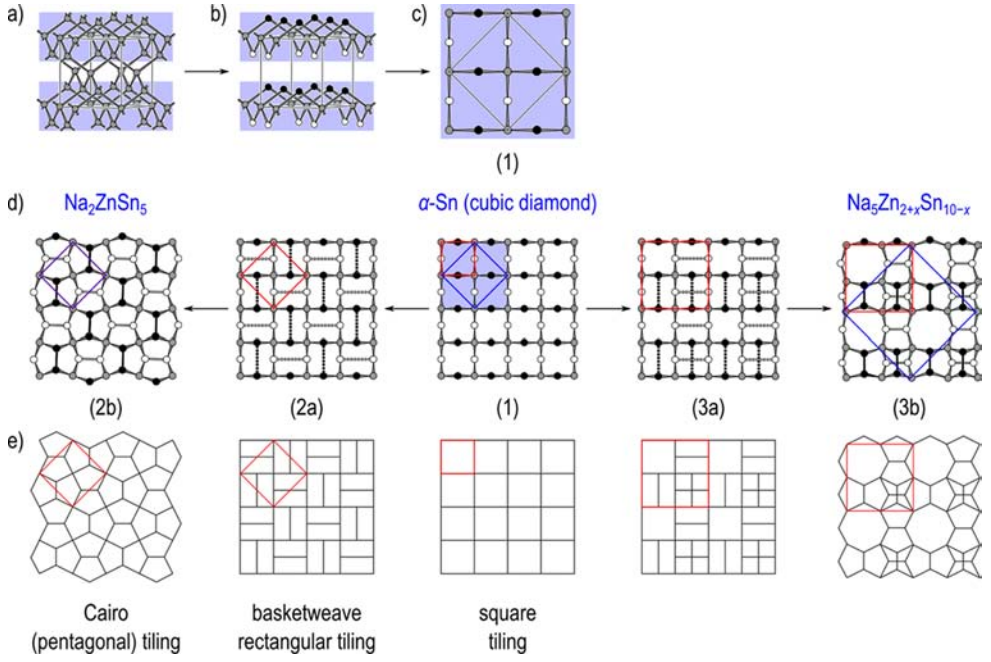

Figure 7. Structural relations between a section of the cubic diamond structure and the layers in the Zn−Sn structural parts of the Na_2ZnSn_5 polymorphs and $Na_5Zn_{2+x}Sn_{10-x}$: (a) cubic diamond structure; (b) two-dimensional section of the cubic diamond structure, layer (1) of four- and two-connected atoms (shown with gray and black or white circles, respectively); (c) top view of such a layer (broken off bonds are not shown); (d) schematic distortion of layer (1) to layers as they occur in the Na_2ZnSn_5 polymorphs (left) and $Na_5Zn_{2+x}Sn_{10-x}$ (right) shown in projection along the stacking directions; (e) related tessellations of the plane. Red squares show the repeating units of the layers and tessellations, respectively, and blue squares indicate the unit cell dimensions of α-Sn, *hP*- and *tI*-Na_2ZnSn_5, and $Na_5Zn_{2+x}Sn_{10-x}$.

dx.doi.org/10.1021/ja401043b | J. Am. Chem. Soc. 2013, 135, 10654−10663

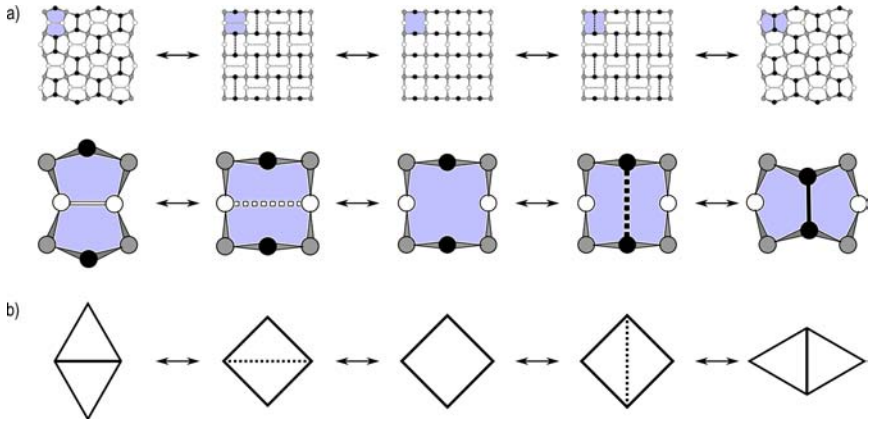

Figure 8. (a) Schematic representations of the rearrangements in a puckered layer of five-membered rings as shown in Figure 5g,h,i. (b) Diamond–square–diamond mechanism.

Table 4. Selected Structural Data for α-Sn, *hP*-Na_2ZnSn_5, *tI*-Na_2ZnSn_5, and $Na_5Zn_{2+x}Sn_{10-x}$

		lattice param/Å			
	space group	parallel to layers	parallel to stacking direction	layers per repeating unit	height of stacking per layer/Å[a]
α-Sn	$Fd\bar{3}m$ (No. 227)	$a = b = 6.49$			
hP-Na_2ZnSn_5	$P6_122$ (No. 178)	orthohexagonal setting:			
		$a' = 6.237$, $b' = 6.451$	$c' = 11.173$	2	$c/2 = 5.59$
tI-Na_2ZnSn_5	$I\bar{4}2d$ (No. 122)	$a = 6.336$	$c = 22.382$	4	$c/4 = 5.60$
$Na_5Zn_{2+x}Sn_{10-x}$	*Pbcn* (No. 60)	$a = 12.772$, $c = 12.777$	$b = 10.804$	2	$b/2 = 5.40$

[a]Lattice parameter parallel to stacking direction divided by number of layers per repeating unit.

Table 5. Selected Structural Data Reported for *hP*-Na_2ZnSn_5, $NaInSn_2$, $NaGaSn_2$, and $NaGaSn_5$ with Analogous Polyanionic Network Structures

formula	space group	absolute config	lattice param/Å	lattice param for orthohexagonal setting[a] or related cell length fraction/Å	ref
Na_2ZnSn_5	$P6_122$ (No. 178)	not determined (enantiomorphic space group: $P6_522$ (No. 179))	$a = 6.451(1)$	$a' = c = 6.237$	this work
				$b' = a = 6.451$	
			$c = 6.237(1)$	$c' = a\sqrt{3} = 11.173$	
$NaInSn_2$	$P2_12_12_1$ (No. 19)	no statement given (Sohncke group)			23
			$a = 6.279(4)$		
			$b = 6.543(2)$		
			$c = 11.396(2)$	$c/\sqrt{3} = 6.579$	
$NaGaSn_2$	$C222_1$ (No. 20)	slightly higher *R* values for other enantiomer (Sohncke group)			22
			$c = 6.162(2)$		
			$a = 6.309(3)$		
			$b = 10.986(4)$	$b/\sqrt{3} = 6.343$	
$NaGaSn_5$	$P3_112$ (No. 151)	not determined (enantiomorphic space group: $P3_212$ (No. 153))			24
			$a = 6.328(4)$	$a' = c = 6.170$	
				$b' = a = 6.328$	
			$c = 6.170(3)$	$c' = a\sqrt{3} = 10.960$	

[a]For the hexagonal or trigonal structures lattice parameters for an orthohexagonal setting are given for comparison. For the orthorhombic structures the given cell length fraction reveals the deviation from hexagonal metrics.

of *hP*-Na_2ZnSn_5 (and the related known Na–*Tr*–Sn phases) as a possible allotrope structure for C,[10,48] Si,[8,10,11,48] Ge,[8,10] and Sn.[10] The network structure of $Na_5Zn_{2+x}Sn_{10-x}$ was recently discovered for the novel open tetrahedral framework of B and Si atoms of the new Zintl phase $LiBSi_2$, which hosts Li atoms in channels of the network.[49]

In this view, also the frameworks of *tI*-Na_2ZnSn_5 and $Na_5Zn_{2+x}Sn_{10-x}$ and other framework structures of four-bonded atoms which can be described according to the building scheme outlined in Figure 7 represent promising candidates for new group 14 element allotrope structures.

■ ASSOCIATED CONTENT

Supporting Information

Text, tables, CIF files, and figures giving details for the DTA experiment and a graph showing the measured DTA curves, powder XRD patterns from temperature-dependent measurements of a sample of *tI*-Na_2ZnSn_5, details for the high-temperature single-crystal XRD measurement and data analysis, details on the ordered model structures for *hP*-Na_2ZnSn_5 and *tI*-Na_2ZnSn_5, further results of electronic structure calculations, including total and partial density of states curves for the ordered model for *hP*-Na_2ZnSn_5, isosurface representations of

the electron localization functions (ELF) for the model for *t*I-Na_2ZnSn_5 and for the model based on *h*P-Na_2ZnSn_5, a discussion of the chemical bonding for Na_2ZnSn_5 in terms of the ELF analyses, and a summary of the group−subgroup relations between the space groups reported for *h*P-Na_2ZnSn_5, $NaInSn_2$, $NaGaSn_2$, and $NaGaSn_5$. This material is available free of charge via the Internet at http://pubs.acs.org.

AUTHOR INFORMATION

Corresponding Author

*E-mail: Thomas.Faessler@lrz.tum.de.

Notes

The authors declare no competing financial interest.

ACKNOWLEDGMENTS

We thank B. Wahl for discussions on the crystal structure analyses and F. Krause, who carried out experimental work on the synthesis of the intermetallic phases.

REFERENCES

(1) Grüttner, A.; Nesper, R.; von Schnering, H. G. *Angew. Chem., Int. Ed. Engl.* **1982**, *21*, 912.
(2) Kiefer, F.; Karttunen, A. J.; Döblinger, M.; Fässler, T. F. *Chem. Mater.* **2011**, *23*, 4578.
(3) Guloy, A. M.; Ramlau, R.; Tang, Z.; Schnelle, W.; Baitinger, M.; Grin, Y. *Nature* **2006**, *443*, 320.
(4) Fässler, T. F. *Angew. Chem., Int. Ed.* **2007**, *46*, 2572; *Angew. Chem.* **2007**, *119*, 2624.
(5) For a recent overview of Ge modifications that have been obtained from high-pressure experiments, also including more examples for network structures with four-bonded atoms, see e.g.: Schwarz, U.; Wosylus, A.; Böhme, B.; Baitinger, M.; Hanfland, M.; Grin, Y. *Angew. Chem., Int. Ed.* **2008**, *47*, 6790.
(6) Nesper, R.; Vogel, K.; Blöchl, P. E. *Angew. Chem., Int. Ed. Engl.* **1993**, *32*, 701; *Angew. Chem.* **1993**, *105*, 786.
(7) Chadi, D. J. *Phys. Rev. B* **1985**, *32*, 6485.
(8) Conesa, J. C. *J. Phys. Chem. B* **2002**, *106*, 3402.
(9) Karttunen, A. J.; Fässler, T. F.; Linnolahti, M.; Pakkanen, T. A. *Inorg. Chem.* **2011**, *50*, 1733.
(10) Pickard, C. J.; Needs, R. J. *Phys. Rev. B* **2010**, *81*, 014106.
(11) Zwijnenburg, M. A.; Jelfs, K. E.; Bromley, S. T. *Phys. Chem. Chem. Phys.* **2010**, *12*, 8505.
(12) Zhao, Z.; Tian, F.; Dong, X.; Li, Q.; Wang, Q.; Wang, H.; Zhong, X.; Xu, B.; Yu, D.; He, J.; Wang, H.-T.; Ma, Y.; Tian, Y. *J. Am. Chem. Soc.* **2012**, *134*, 12362.
(13) Pöttgen, R.; Dinges, T.; Eckert, H.; Sreeraj, P.; Wiemhöfer, H.-D. *Z. Phys. Chem* **2010**, *224*, 1475.
(14) *Handbook of Battery Materials*, 2nd ed.; Claus, D., Besenhard, J. O., Eds.; Wiley-VCH: Weinheim, Germany, 2011.
(15) Blase, W.; Cordier, G.; Kniep, R. *Z. Anorg. Allg. Chem.* **1993**, *619*, 1161.
(16) Stegmaier, S.; Fässler, T. F. *Inorg. Chem.* **2013**, *52*, 2809.
(17) Bobev, S.; Sevov, S. C. *J. Solid State Chem.* **2000**, *153*, 92.
(18) Nolas, G. S.; Weakley, T. J. R.; Cohn, J. L. *Chem. Mater.* **1999**, *11*, 2470.
(19) Nolas, G. S.; Cohn, J. L.; Dyck, J. S.; Uher, C.; Yang, J. *Phys. Rev. B* **2002**, *65*, 165201.
(20) Wilkinson, A. P.; Lind, C.; Young, R. A.; Shastri, S. D.; Lee, P. L.; Nolas, G. S. *Chem. Mater.* **2002**, *14*, 1300.
(21) Kaltzoglou, A.; Ponou, S.; Fässler, T. F. *Eur. J. Inorg. Chem.* **2008**, 538.
(22) Vaughey, J. T.; Corbett, J. D. *J. Am. Chem. Soc.* **1996**, *118*, 12098.
(23) Blase, W.; Cordier, G.; Kniep, R.; Schmidt, R. *Z. Naturforsch., B* **1989**, *44*, 505.
(24) Blase, W.; Cordier, G. Z. *Naturforsch., B* **1988**, *43*, 1017.
(25) Ponou, S.; Kim, S.-J.; Fässler, T. F. *J. Am. Chem. Soc.* **2009**, *131*, 10246.
(26) *WinXPOW (Version 2.08)*; STOE & Cie GmbH, Darmstadt, Germany, 2003.
(27) Rodriguez-Carvajal, J. *FullProf Suite*; 2009.
(28) Rodriguez-Carvajal, J. *FullProf.2k (Version 4.80)*; 2010.
(29) Rodriguez-Carvajal, J.; Roisnel, T. *WinPLOTR*; 2010.
(30) *CrysAlis RED (Version 1.171.33.34d)*; Oxford Diffraction Ltd., 2009.
(31) *X-RED32 (Version 1.26)*, STOE & Cie GmbH, Darmstadt, Germany, 2004.
(32) *X-SHAPE (Version 2.05)*; STOE & Cie GmbH, Darmstadt, Germany, 2004.
(33) *XPREP (Version 6.14)*; Bruker Nonius, 2003.
(34) *XS - Crystal Structure Solution - SHELXTL (Version 6.12)*; Bruker AXS, 2001.
(35) Sheldrick, G. *Acta Crystallogr., Sect. A* **2008**, *64*, 112.
(36) *XL - Crystal Structure Refinement - SHELXTL (Version 6.12)*; Bruker AXS, 2001.
(37) Gelato, L. M.; Parthe, E. *J. Appl. Crystallogr.* **1987**, *20*, 139.
(38) Spek, A. L. *Acta Crystallogr., Sect. A* **1990**, *46*, c34.
(39) Jepsen, O.; ; Burkhardt, A.; ; Andersen, O. K. *The Stuttgart TB-LMTO-ASA Program (Version 4.7)*; Max-Planck-Institut für Festkörperforschung, Stuttgart, Germany, 1998.
(40) Barth, U. V.; Hedin, L. *J. Phys. C: Solid State Phys.* **1972**, *5*, 1629.
(41) Blöchel, P. E.; Jepsen, O.; Andersen, O. K. *Phys. Rev. B* **1994**, *49*, 16223.
(42) Momma, K.; Izumi, F. *J. Appl. Crystallogr.* **2008**, *41*, 653.
(43) Fässler, T. F.; Kronseder, C. *Angew. Chem., Int. Ed.* **1998**, *37*, 1571; *Angew. Chem.* **1999**, *110*, 1641.
(44) Evers, J.; Oehlinger, G.; Sextl, G.; Becker, H.-O. *Angew. Chem., Int. Ed. Engl.* **1987**, *26*, 76.
(45) Fässler, T. F. *Coord. Chem. Rev.* **2001**, *215*, 347.
(46) Lipscomb, W. N. *Science* **1966**, *153*, 373.
(47) The network was recognized (in ref 10) as related to a hypothetical zeolite structure that was enumerated 271 and identified as chemically feasible in: Foster, M. D.; Delgado Friedrichs, O.; Bell, R. G.; Almeida Paz, F. A.; Klinowski, J. *J. Am. Chem. Soc.* **2004**, *126*, 9769.
(48) Connétable, D. *Phys. Rev. B* **2011**, *83*, 035206.
(49) Zeilinger, M.; van Wüllen, L.; Benson, D.; Kranak, V. F.; Konar, S.; Fässler, T. F.; Häussermann, U. *Angew. Chem., Int. Ed.* **2013**, *52*, 5978; *Angew. Chem.* **2013**, *125*, 6094.